Two-dimensional SU(N) gauge theory on the light cone

Takanori Sugihara*
Department of Physics, Kyushu University, Fukuoka 812, Japan

Masayuki Matsuzaki†
Department of Physics, Fukuoka University of Education, Fukuoka 811-41, Japan

Masanobu Yahiro‡
Shimonoseki University of Fisheries, Shimonoseki 759-65, Japan
(Received 23 February 1994)

Two-dimensional SU(N) gauge theory is accurately analyzed with the light-front Tamm-Dancoff approximation, both numerically and analytically. The light-front Einstein-Schrödinger equation for the mesonic mass is reduced to the 't Hooft equation in the large N limit with g^2N fixed, where g is the coupling constant. Two mesonic and one baryonic bound states are obtained numerically in the region of $g^2N \gg m^2$ for small N, where m is the bare quark (q) mass. The lightest meson and the baryon consist predominantly of valence quarks. The second mesonic state is highly relativistic in the sense that it has a large four-body ($qq\bar{q}\bar{q}$) component in addition to the valence ($q\bar{q}$) one. Our results are consistent with results of the lattice calculation for SU(2) and also with the prediction of bosonization for ratios of the two mesonic masses to the baryonic one in the strong coupling limit. Analytic solutions to the lightest hadronic masses are obtained, with a reasonable approximation, as $\sqrt{2Cm}(1-1/N^2)^{1/4}$ for the meson and $\sqrt{CmN(N-1)}(1-1/N^2)^{1/4}$ for the baryon, where $C=(g^2N\pi/6)^{1/2}$. The solutions well reproduce the numerical ones. The N and m dependences of the hadronic masses are explicitly shown by the analytical solutions.

PACS number(s): 11.10.Kk, 11.15.Pg, 11.15.Tk

I. INTRODUCTION AND SUMMARY

Two-dimensional SU(N) quantum chromodynamics [QCD(N)$_2$] is a good model for studying ideas and tools, which are expected to be feasible in analyses of QCD in 3+1 dimensions. 't Hooft introduced the model to test the power of the $1/N$ expansion [1]. He summed planar diagrams, which dominate the leading order in the expansion and derived an equation. The 't Hooft equation is valid in the large N limit with g^2N fixed, where g is the coupling constant. The mass spectrum of the equation reveals a nearly straight "Regge trajectory."

The large N limit corresponds to the weak coupling one, since g^2N is fixed. The $1/N$ expansion then works in the weak coupling regime ($g \ll m$, m being the bare quark mass), but not in the strong coupling one because it is almost impossible to calculate higher-order terms in the expansion. For this reason, QCD(N)$_2$ in the strong coupling regime has been studied with some other methods so far. Nevertheless, the dynamics is not understood well in the region. The bosonization predicts ratios of meson masses to a baryon mass [2], but they are valid only in the strong coupling limit. The lattice calculation has given a low-energy spectrum of SU(2), but their accuracy is poor [3,4].

The discretized light-cone quantization (DLCQ) has been proposed as a useful tool for computing hadronic masses [5–9]. The mass obtained with DLCQ is a function of K, the parameter, which characterizes the discretization of the total light-cone momentum $\mathcal{P}$. One then has to take the large K limit to get physical masses containing no unphysical parameter, but the convergence is very slow for large g [6]. Increasing K demands a lot of numerical efforts, so that a reasonably large K was not taken in calculations done so far for strong coupling [7].

Recently the light-front Tamm-Dancoff (LFTD) approximation [10] has been proposed as one of the alternative nonperturbative tools to lattice gauge theory. In the standard equal-time field theory the vacuum state is an infinite sea of constituents [quarks (q) and gluons in QCD] and hadrons arise as excitations of the sea. It is then unlikely that the vacuum and the hadrons are well described with a finite number of constituents. In fact, such a truncation of the Fock space, i.e., the Tamm-Dancoff approximation [11], causes some serious problems [10]. Such problems do not appear in light-front field theory [12], owing to the fact that the vacuum is trivial on the light cone [10]. The LFTD approximation is the Tamm-Dancoff approximation applied to light-front field theory. Both LFTD and DLCQ are based on light-front field theory, but LFTD seems more reliable than DLCQ at strong coupling [13].

On the other hand, LFTD has its own problems: (a)

*Electronic address: sugi1scp@mbox.nc.kyushu-u.ac.jp
†Electronic address: matsuza@fukuoka-edu.ac.jp
‡Electronic address: c74418x@kyu-msp.cc.kyushu-u.ac.jp

nonperturbative renormalization, (b) the relation between spontaneous symmetry breaking and the triviality of the vacuum (what is called, the "zero-mode" problem), and (c) recovery of rotational symmetry. These essential problems have not been settled yet. However, they would not appear in two-dimensional models such as QCD$(N)_2$. Coleman's theorem [14] says that any breaking of global continuous symmetry does not occur in two dimensions. We then do not face the problem (b). The problems (a) and (c) do not exist, from the outset, in two dimensions.

In this paper, we study QCD$(N)_2$ in the region of $g^2N \gg m^2$ with LFTD; the region corresponds to the strong coupling region ($g \gg m$) for small N, and for large N it covers not only the strong coupling region but also the medium and weak coupling ones. We first derive the light-cone Hamiltonian P^- and the Einstein-Schrödinger (ES) equation $2\mathcal{P}P^-|\Psi\rangle = M^2|\Psi\rangle$ for hadronic mass and wave function M and $|\Psi\rangle$ in the framework of the light-front field theory [12]. As the Tamm-Dancoff approximation, the mesonic SU(N) wave function is described with two-body ($q\bar{q}$) and four-body ($qq\bar{q}\,\bar{q}$) states, and the baryonic wave function with the N-body (q^N) state. Inclusion of the four-body state is essential to obtain results (ii) and (iii) mentioned in the next paragraph. The ES equation is numerically solved by diagonalizing P^- within the space spanned by a finite number of basis functions. All tools needed for this calculation are prepared by our previous work [15] for the massive Schwinger model.

Our main results are summarized as follows.

(i) P^- involves a term proportional to Q^2/η, where Q^2 is the Casimir operator of SU(N) and η is an infinitesimal constant. The term enforces confinement, restricting finite-energy solutions to color singlets. This is a well-known property of QCD$(N)_2$.

(ii) In the ES equation the two-body sector is coupled with the four-body one through couplings of order $1/\sqrt{N}$, so that the two-body sector is decoupled from the four-body one in the large N limit. The two-body sector, as expected, tends to the 't Hooft equation in the limit. The four-body sector does not produce any bound state in the limit.

(iii) Two mesonic and one baryonic bound states are obtained numerically for small N. Masses of the three states behave as $m^{1/2}$ at small m, as expected from the partially conserved axial-vector current (PCAC) [15]. The lightest mesonic mass is consistent with the corresponding result of lattice calculations for SU(2), although the calculations contain much larger errors than ours. The lightest meson and the baryon consist predominantly of valence quarks. The second mesonic state is highly relativistic in the sense that it has the $q\bar{q}$ and $qq\bar{q}\,\bar{q}$ components with almost the same magnitude. The existence of such a relativistic state is unpredictable from the diagramatic consideration based on $1/N$ expansion, since the 't Hooft equation as a result of the consideration generates only two-body states. Ratios of the two mesonic masses to the baryonic one at small m agree with the prediction [2] of the bosonization within $\sim 7\%$ error.

(iv) Assuming that the lightest meson and the baryon consist only of valence quarks, we can obtain approximate solutions to their masses as

$$\sqrt{2Cm}(1-1/N^2)^{1/4}$$

for meson and

$$\sqrt{CmN(N-1)}(1-1/N^2)^{1/4}$$

for baryon, where $C = (g^2N\pi/6)^{1/2}$. The approximate solutions are accurate in the region of $g^2N \gg m^2$, since the assumption is quite reliable there. They show the N dependence of the masses explicitly in the whole range of N. The leading in $1/N$ is $O(N^0)$ for the mesonic mass and $O(N)$ for the baryonic one, as expected from topological considerations [16–18] based on the expansion. A theoretical surprise is that the next-to-leading order is not $O(N^{-1})$ but $O(N^{-2})$ for the mesonic mass, since the mass is a function of N^2. This makes the 't Hooft solution more reliable for the lightest mesonic mass.

We derive the light-cone Hamiltonian and result (i) in Sec. II A and the ES equation for hadronic mass and result (ii) in Sec. II C. In Sec. II B the color-singlet states of meson and baryon are constructed within the truncated Fock space. We first present, in Sec. II D, the approximate solutions to the lightest hadronic masses and result (iv). The approximate but analytic solutions are convenient to see the N and m dependences of the masses explicitly. Accuracy of the approximate solutions are tested in Sec. III. Numerical methods and result (iii) are also presented there. Section IV is devoted to discussions. Appendices are collections of lengthy expressions.

II. LIGHT-FRONT TAMM-DANCOFF APPROXIMATION

A. Light-cone Hamiltonian

The Lagrangian density of QCD$(N)_2$ for interacting quark and gauge fields, ψ and A^a_μ ($a = 1$ to N^2-1), is

$$\mathcal{L} = -\tfrac{1}{4}F^a_{\mu\nu}F^{a\mu\nu} + \bar{\psi}(i\gamma^\mu D_\mu - m)\psi, \tag{2.1}$$

where $D_\mu = \partial_\mu - igA^a_\mu T^a$ and $F^a_{\mu\nu} = \partial_\mu A^a_\nu - \partial_\nu A^a_\mu + gf_{abc}A^b_\mu A^c_\nu$ for the generator T^a and the structure constant f_{abc} of SU(N). Light-front field theory [12] starts with the introduction of light-cone coordinates:

$$x^\mu = (x^+, x^-) \equiv ((x^0 + x^1)/\sqrt{2}, (x^0 - x^1)/\sqrt{2});$$

for any other vector, $V^\pm = (V^0 \pm V^1)/\sqrt{2}$. (We take the same notation and conventions as in Ref. [15].) The equations of motion are

$$\begin{aligned} i\sqrt{2}\partial_- \psi_L &= m\psi_R, \\ i\sqrt{2}\partial_+ \psi_R &= m\psi_L - \sqrt{2}gA^-\psi_R, \\ \partial_-^2 A^{a-} &= \sqrt{2}g\psi_R^\dagger T^a \psi_R, \\ -\partial_-\partial_+ A^{a-} &= \sqrt{2}g\psi_L^\dagger T^a \psi_L + gf_{abc}A^{b-}\partial_- A^{c-} \end{aligned} \tag{2.2}$$

for the light-cone gauge, $A^{a+} = 0$, where $\psi = (\psi_R, \psi_L)^T$. The first and third equations do not involve the time derivative (∂_+) and are therefore just constraints, which determine ψ_L and A^- in terms of ψ_R. Thus, ψ_L and A^- are not independent variables and not subject to a quantization condition. The constraints are then solved with the inverse derivative operator ∂_-^{-1}:

$$\psi_L(x^-) = -i\frac{m}{\sqrt{2}}\frac{1}{\partial_-}\psi_R$$
$$= -i\frac{m}{2\sqrt{2}}\int dy^-\epsilon(x^- - y^-)\psi_R(y^-), \quad (2.3)$$

$$A^{a-}(x^-) = \sqrt{2}g\frac{1}{\partial_-^2}\psi_R^\dagger(x^-)T^a\psi_R(x^-), \quad (2.4)$$

where $\epsilon(x)$ is 1 for $x > 0$ and -1 for $x < 0$. The only independent variable ψ_R is quantized by an anticommutation relation at the equal light-cone time $x^+ = y^+$,

$$\{\psi_{iR}(x), \psi_{jR}^\dagger(y)\}_{x^+=y^+} = \frac{1}{\sqrt{2}}\delta_{ij}\delta(x^- - y^-). \quad (2.5)$$

Adopting the light-cone coordinates and light-cone gauge thus reduces a number of independent variables. This is an advantage of light-front field theory. The energy-momentum vectors commute mutually and are therefore constants of motion. The time component (light-cone Hamiltonian) is

$$P^- = -\frac{im^2}{2\sqrt{2}}\int dx^- dy^-\psi_R^\dagger(x^-)\epsilon(x^- - y^-)\psi_R(y^-)$$
$$-\frac{g^2}{2}\int dx^- j^{a+}(x^-)\frac{1}{\partial_-^2}j^{a+}(x^-), \quad (2.6)$$

and the spatial one (light-cone momentum) is

$$P^+ = i\sqrt{2}\int dx^-\psi_R^\dagger(x^-)\partial_-\psi_R(x^-). \quad (2.7)$$

The field ψ_R is expanded at $x^+ = 0$ in terms of free waves [19], each with momentum k^+:

$$\psi_{iR}(x^-) = \frac{1}{2^{1/4}}\int_0^\infty \frac{dk^+}{2\pi\sqrt{k^+}}[b_i(k^+)e^{-ik^+x^-}$$
$$+d_i^\dagger(k^+)e^{ik^+x^-}], \quad (2.8)$$

with

$$\{b_i(k^+), b_j^\dagger(l^+)\} = \{d_i(k^+), d_j^\dagger(l^+)\}$$
$$= 2\pi k^+\delta_{ij}\delta(k^+ - l^+). \quad (2.9)$$

The color current $j^{a+} \equiv \sqrt{2}{:}\psi_R^\dagger T^a\psi_R{:}$ is normal ordered with respect to the creation and annihilation operators. The charge is then

$$Q^a = \int dx^- j^{a+}$$
$$= \sum_{i,j}^N (T^a)_{ij}\int_0^\infty \frac{dk^+}{2\pi k^+}[b_i^\dagger(k^+)b_j(k^+)$$
$$-d_j^\dagger(k^+)d_i(k^+)]. \quad (2.10)$$

The last term in P^- can be rewritten with the standard Fourier transform [20],

$$\int dx_1^- j^{a+}(x_1^-)\frac{1}{\partial_-^2}j^{a+}(x_1^-) = \frac{1}{4}\int dx_1^- dx_2^- dy^- j^{a+}(x_1^-)\epsilon(x_1^- - y^-)\epsilon(y^- - x_2^-)j^{a+}(x_2^-)$$
$$= \frac{1}{2}\int dx_1^- dx_2^- j^{a+}(x_1^-)|x_1^- - x_2^-|j^{a+}(x_2^-) - \frac{1}{4\eta}\sum_{a=1}^{N^2-1}Q^aQ^a + O(\eta), \quad (2.11)$$

where use has been made of

$$\epsilon(x) = \frac{1}{2\pi i}\int_{-\infty}^\infty dk\left(\frac{1}{k+i\eta} + \frac{1}{k-i\eta}\right)e^{ikx}, \quad (2.12)$$

$$|x| = \frac{1}{2\pi i^2}\int_{-\infty}^\infty dk\left[\frac{1}{(k+i\eta)^2} + \frac{1}{(k-i\eta)^2}\right]e^{ikx}. \quad (2.13)$$

The term $Q^2/4\eta(Q^2 \equiv \sum Q^aQ^a)$ enforces confinement, restricting finite eigenvalues to the color-singlet ($Q^2 = 0$) subspace.

The Hamiltonian is expressed with the creation and annihilation operators,

$$P^- = P^-_{\text{free}} + P^-_{\text{self}} + P^-_0 + P^-_2,$$

$$P^-_{\text{free}} = \frac{m^2}{4\pi}\sum_{i=1}^N\int_0^\infty\frac{dk}{k^2}[b_i^\dagger(k)b_i(k) + d_i^\dagger(k)d_i(k)],$$

$$P^-_{\text{self}} = \frac{g^2}{8\pi^2}\sum_{a=1}^{N^2-1}\sum_{i,j,k,l}^N(T^a)_{ij}(T^a)_{kl}\int_0^\infty\frac{dk_1}{k_1}\delta_{jk}[b_i^\dagger(k_1)b_l(k_1) + d_l^\dagger(k_1)d_i(k_1)]\int_0^\infty dk_2\left[\frac{1}{(k_1-k_2)^2} - \frac{1}{(k_1+k_2)^2}\right], \quad (2.14)$$

$$P^-_0 = \frac{g^2}{8\pi^3}\sum_{a=1}^{N^2-1}\sum_{i,j,k,l}^N(T^a)_{ij}(T^a)_{kl}\int_0^\infty\prod_{m=1}^4\frac{dk_m}{\sqrt{k_m}}\delta(k_1+k_2-k_3-k_4)$$
$$\times\left\{[b_i^\dagger(k_1)b_k^\dagger(k_2)b_l(k_3)b_j(k_4) + d_j^\dagger(k_1)d_l^\dagger(k_2)d_k(k_3)d_i(k_4)]\frac{1}{2(k_1-k_4)^2}\right.$$
$$\left.-b_i^\dagger(k_1)d_l^\dagger(k_2)d_k(k_3)b_j(k_4)\frac{1}{(k_1-k_4)^2} + b_i^\dagger(k_1)d_j^\dagger(k_2)d_k(k_3)b_l(k_4)\frac{1}{(k_1+k_2)^2}\right\},$$

$$P^-_2 = \frac{g^2}{8\pi^3}\sum_{a=1}^{N^2-1}\sum_{i,j,k,l}^N(T^a)_{ij}(T^a)_{kl}\int_0^\infty\prod_{m=1}^4\frac{dk_m}{\sqrt{k_m}}\frac{\delta(k_1+k_2+k_3-k_4)}{(k_1-k_4)^2}$$
$$\times[b_i^\dagger(k_1)b_k^\dagger(k_2)d_l^\dagger(k_3)b_j(k_4) + b_i^\dagger(k_4)d_k(k_3)b_l(k_2)b_j(k_1) + d_j^\dagger(k_1)d_l^\dagger(k_2)b_k^\dagger(k_3)d_i(k_4) + d_j^\dagger(k_4)b_l(k_3)d_k(k_2)d_i(k_1)],$$

where the integration stands for the Cauchy's principal-value one. The Hamiltonian does not involve any term having the creation operators only or the annihilation ones only. This indicates that the Fock vacuum is an eigenstate of P^-, i.e., a true vacuum. The property of the Hamiltonian stems from the conservation of the total light-cone momentum. Each particle must have either zero or a positive momentum, as shown in Eq. (2.8). The creation or the annihilation of particles, each with positive k^+, breaks the conservation. An exception is the zero mode ($k^+ = 0$): Only the mode can make the true vacuum nontrivial without breaking the conservation. The mode is thus responsible for nontrivial structure of vacua such as spontaneous symmetry breaking. In the present model, however, the mode is prohibited as long as $m \neq 0$, because the mass term in $P^-_{\rm free}$ enforces the eigenstate of P^- to vanish at $k^+ = 0$ [21].

There appears a force, $b_i^\dagger(k_1)d_i^\dagger(k_2)b_j(k_3)d_j(k_4)$, in P_0^-, after the summation is made over a. The force is considered to be induced by the so-called annihilation diagrams where a q-$\bar{q}$ pair annihilates into an instantaneous gluon at a vertex, while another pair is created at the second vertex. Further discussion will be made in Sec. IV.

B. Hadronic color-singlet states

The conserved color charges Q^a ($a = 1, 2, \ldots, N^2 - 1$) are generators of SU($N$). These can be recombined into $N - 1$ operators being mutually commutable and $N(N-1)/2$ pairs of raising and lowering operators. Whenever these operators act on color-singlet states, the value is always zero. Using the condition, one can easily construct color-singlet states of the meson and baryon:

$$|\Psi_{\rm meson}\rangle = |{\rm meson}\rangle_2 + |{\rm meson}\rangle_4, \tag{2.15}$$

$$|{\rm meson}\rangle_2 = \frac{1}{\sqrt{N}} \int_0^{\mathcal{P}} \frac{dk_1 dk_2}{2\pi\sqrt{k_1 k_2}} \delta(\mathcal{P} - k_1 - k_2)\psi_2(k_1, k_2) \sum_{m=1}^{N} b_m^\dagger(k_1) d_m^\dagger(k_2)|0\rangle, \tag{2.16}$$

$$\begin{aligned} |{\rm meson}\rangle_4 = \frac{1}{\sqrt{2N(N+1)}} \int_0^{\mathcal{P}} \prod_{i=1}^{4} \frac{dk_i}{\sqrt{2\pi k_i}} \delta\left(\mathcal{P} - \sum_{i=1}^{4} k_i\right) \\ \times \Bigg\{ \psi_A(k_1, k_2, k_3, k_4) \sum_{m=1}^{N} b_m^\dagger(k_1) d_m^\dagger(k_2) b_m^\dagger(k_3) d_m^\dagger(k_4) \\ + \left[\psi_A(k_1, k_2, k_3, k_4) + \left(\frac{N+1}{N-1}\right)^{1/2} \psi_S(k_1, k_2, k_3, k_4) \right] \\ \times \sum_{m \neq n}^{N} b_m^\dagger(k_1) d_m^\dagger(k_2) b_n^\dagger(k_3) d_n^\dagger(k_4) \Bigg\} |0\rangle, \end{aligned} \tag{2.17}$$

$$|\Psi_{\rm baryon}\rangle = \int_0^{\mathcal{P}} \delta\left(\mathcal{P} - \sum_{i=1}^{4} k_i\right) \psi_b(k_1, k_2, \ldots, k_N) \prod_{i=1}^{N} \frac{dk_i}{\sqrt{2\pi k_i}} b_1^\dagger(k_1) \cdots b_N^\dagger(k_N)|0\rangle, \tag{2.18}$$

where each wave function has a symmetry for an interchange of two momenta,

$$\begin{aligned} \psi_A(k_1, k_2, k_3, k_4) &= -\psi_A(k_3, k_2, k_1, k_4) \\ &= -\psi_A(k_1, k_4, k_3, k_2), \end{aligned} \tag{2.19}$$

$$\begin{aligned} \psi_S(k_1, k_2, k_3, k_4) &= \psi_S(k_3, k_2, k_1, k_4) \\ &= \psi_S(k_1, k_4, k_3, k_2), \end{aligned} \tag{2.20}$$

$$\psi_b(\ldots, k_i, \ldots, k_j, \ldots) = \psi_b(\ldots, k_j, \ldots, k_i, \ldots) \tag{2.21}$$

for any i and j. The color-singlet states are expanded in terms of the number of quarks and antiquarks, and truncated to the two- and four-body components for the mesonic state and to the N-body one for the baryonic state. The Q^a's do not couple a truncated space with the remainder, so they keep proper commutation relations between them within the truncated space. The truncation, i.e., the Tamm-Dancoff approximation [11], thus does not break SU(N) symmetry.

C. Light-front Einstein-Schrödinger (ES) equation for hadronic mass

The ES equation for hadronic mass is $2\mathcal{P}P^-|\Psi\rangle = M^2|\Psi\rangle$ in the light-front form, where P^+ has been replaced by its eigenvalue $\mathcal{P}$ as a constant of motion. In the equation, $\mathcal{P}$ can be scaled out by changing variables k_i into their fractions $x_i = k_i/\mathcal{P}$: The

two- and four-body wave functions, $\psi_2(k_1,k_2)$ and $\psi_4(k_1,k_2,k_3,k_4)$, are also replaced by $\psi_2(x_1,x_2)$ and $\psi_4(x_1,x_2,x_3,x_4)/\mathcal{P}$ in $|\Psi_{\rm meson}\rangle$, while $\psi_b(k_1,\ldots,k_N)$ by $\psi_b(x_1,\ldots,x_N)/\mathcal{P}^{N/2-1}$ in $|\Psi_{\rm baryon}\rangle$. Left multiplying the rescaled equation by individual bases of the truncated Fock space leads to a set of coupled equations for the wave functions. In the mesonic case, the equations are lengthy and then presented in Appendix A. Couplings between the two- and four-body sectors of the equations are of order $1/\sqrt{N}$ in $1/N$, where g^2N is fixed. In the large N limit, the two-body sector is then decoupled from the four-body one, and the two-body sector tends to the 't Hooft equation. (This discussion is even clearer in the matrix representation of the coupled equations in Appendix C.) This conclusion is not changed by further inclusion of six-body states, since the resultant equations involve no direct coupling between the two- and six-body sectors. According to numerical calculations done in Sec. III, the decoupled four-body sector does not produce any bound state. All the bound states in the large N limit thus appear as two-body states.

To see the behavior of mesonic mass in the massless limit ($m/g \to 0$), we integrate Eq. (A1) over x,

$$M^2\int_0^1 dx\,\psi_2(x,1-x) = m^2\int_0^1 dx\left(\frac{1}{x}+\frac{1}{1-x}\right)\times\psi_2(x,1-x), \quad (2.22)$$

where all interaction terms have been completely canceled to each other. The equation shows that $M=0$ and/or $\int\psi_2\,dx = 0$ at $m=0$. The first condition says that the ground-state mass is zero because M must be equivalent to or larger than 0, and the second one that all excited states giving positive M are orthogonal to 1. Only a state orthogonal to all excited states is the ground state, so $\psi_2 = 1$ for the ground state. When $\psi_2 = 1$, all couplings between the two- and four-body sectors of Eq. (A1) vanish, so that $\psi_A = \psi_S = 0$. It turns out that $M=0$ and $\psi_2 = 1$ and $\psi_A = \psi_S = 0$ for the ground state. This fact suggests that the ground state has small four-body components in the region of $m^2 \ll g^2N$. This will be supported by numerical tests in Sec. III.

The equation for the baryonic wave function ψ_b is

$$M^2\psi_b(x_1,x_2,\ldots,x_N) = \left(m^2-\frac{N^2-1}{2N}\frac{g^2}{\pi}\right)\left(\sum_{i=1}^N\frac{1}{x_i}\right)\psi_b(x_1,x_2,\ldots,x_N) - \frac{N+1}{2N}\frac{g^2}{\pi}\int_0^1 dy_1\,dy_2\sum_{i>j}^N\frac{\delta(x_i+x_j-y_1-y_2)}{(x_i-y_1)^2}\psi_b(x_1,\ldots,y_1,\ldots,y_2,\ldots,x_N), \quad (2.23)$$

where $\sum_{i=1}^N x_i = 1$ and the ith and jth arguments of ψ_b in the second term have been replaced by y_1 and y_2, respectively. The equation is reduced to a form similar to Eq. (2.22), when it is integrated over all x_i. The same form is still derivable, even if the truncated space is extended up to the $(N+2)$-body state ψ_{N+2}; this is shown explicitly in Appendix A for the case of SU(2). The baryonic mass as well as the mesonic one thus vanishes in the massless limit, as far as the ground state is concerned. The baryonic wave function is then $\psi_b = 1$ and $\psi_{N+2} = 0$. Just like the mesonic case, this implies that ψ_{N+2} nearly equals to 0 in the region of $m^2 \ll g^2N$. For this reason, only the valence (N-body) state will be taken into account in numerical calculations done in Sec. III.

Burkardt calculated structure functions of the lightest SU(2) meson and baryon with LFTD retaining only of valence quarks [22]. This valence quark approximation is considered to be good for small m^2/g^2N from the consideration mentioned above on the behavior of the lightest mesonic and baryonic states near the massless limit (the strong coupling limit). This is justified also by numerical calculations retaining not only the valence state but also the higher Fock state, as shown in Sec. III B.

D. Approximate solutions to the lightest hadronic masses

The two-body sector of the coupled equations for mesonic wave functions coincides with the corresponding one in the massive Schwinger model, except for a factor $N(1-1/N^2)$ and a term $\int_0^1 dx\,\psi(x,1-x)$ irrelevant to the following statement. Bergknoff [21] showed in the massive Schwinger model that the term in P^- involving m enforces $\psi_2(0) = \psi_2(1) = 0$. Following his analysis, we can determine the behavior of ψ_2 near $x=0$ and 1 as $[x(1-x)]^\beta$ with

$$2\pi m^2/[g^2N(1-1/N^2)] - 1 + \pi\beta\cot(\pi\beta) = 0, \quad (2.24)$$

where it is assumed that

$$2\pi m^2/[g^2N(1-1/N^2)] \ll 1.$$

In the massless limit $[x(1-x)]^\beta$ tends to 1, that is, the exact solution at $m=0$, because of $\beta = 0$ there. This strongly implies that $[x(1-x)]^\beta$ is a good approximation to $\psi_2(x)$ at all x, as long as $2\pi m^2/[g^2N(1-1/N^2)] \ll 1$. This will be supported by numerical tests in Sec. III. The same discussion can be made for baryon. Inserting $\psi_2(x) = [x(1-x)]^\beta$ into Eq. (2.22), one can obtain a mass of the lightest meson approximately as

$$\left[2Cm\left(1-\frac{1}{N^2}\right)^{1/2}\right]^{1/2}, \quad (2.25)$$

where $C = (g^2N\pi/6)^{1/2}$. A mass of the lightest baryon is also obtained in a similar way as

$$\left[CmN(N-1)\left(1-\frac{1}{N^2}\right)^{1/2}\right]^{1/2}, \quad (2.26)$$

The approximate solutions show m- and N dependences of M explicitly.

In a $1/N$ expansion of the solutions, the leading order is $O(N^0)$ for the mesonic mass and $O(N)$ for the baryonic mass, as expected from topological considerations [16–18]. As an interesting result, the next-to-leading order is not $O(N^{-1})$ but $O(N^{-2})$ for the mesonic mass because the mass is an even function of N. This makes the $1/N$ expansion more reliable especially for the lightest mesonic mass. This is not the case for other mesonic states and the baryonic one.

The approximate solutions also indicate that the hadronic masses behave like $m^{1/2}$ at small m. This behavior is also seen in the massive Schwinger model with two flavors [15]. As a result of the behavior, the "pion" decay constant becomes really a constant, indicating that PCAC is a valid concept even for the toy model. This is true also for the present model.

III. NUMERICAL METHOD AND RESULTS

A. Basis functions

The truncated ES equations for hadron masses are numerically solved with the variational method: The wave functions are expanded in terms of basis functions, and the coefficients of expansion are determined by diagonalizing P^- in the space spanned by the basis functions. All tools needed for computations are shown in Ref. [15].

A reasonable choice of the basis functions is

$$\psi_2(x,1-x)=\sum_{n=0}^{N_2} a_n f_n(x), \tag{3.1}$$

$$\psi_A(x_1,x_2,x_3,x_4)=\sum_{n=0}^{N_4} b_n G_n(x_1,x_2,x_3,x_4), \tag{3.2}$$

$$\psi_S(x_1,x_2,x_3,x_4)=\sum_{n=0}^{N_4} c_n G_n(x_1,x_2,x_3,x_4), \tag{3.3}$$

$$\psi_b(x_1,\ldots,x_N)=\sum_{n=0}^{N_b} d_n F_n(x_1,\ldots,x_N) \tag{3.4}$$

with

$$f_n=\begin{cases}[x(1-x)]^{\beta+n}, \\ [x(1-x)]^{\beta+n}(2x-1),\end{cases} \tag{3.5}$$

$$G_n=\begin{cases}(x_1x_2x_3x_4)^\beta(x_{13}^-)^{n_1}(x_{13}^+x_{24}^+)^{n_2}(x_{24}^-)^{n_3}, \\ (x_1x_2x_3x_4)^\beta(x_{13}^-)^{n_1}(x_{13}^+x_{24}^+)^{n_2}(x_{24}^-)^{n_3}x_{13}^+,\end{cases} \tag{3.6}$$

for all N and

$$F_n(x,1-x)=[x(1-x)]^{\beta+n} \tag{3.7}$$

for SU(2) and

$$F_n(x_1,x_2,x_3)=\begin{cases}(x_1x_2x_3)^\beta\mathcal{S}[(x_{12}^-)^{n_1}(x_{12}^+)^{n_1}x_3^{n_2}], \\ (x_1x_2x_3)^\beta\mathcal{S}[(x_{12}^-)^{n_1}(x_{12}^+)^{n_1}x_3^{n_2+1}],\end{cases} \tag{3.8}$$

for SU(3), where $\sum x_i=1$ for each basis function, $x_{ij}^\pm=x_i\pm x_j$ and $\mathcal{S}$ is the symmetrizer. The subscript n of G_n stands for a set (n_1,n_2,n_3), and for other functions analogously. As already discussed in Sec. II D, f_0 (F_0) is a good approximation to the exact ψ_2 (ψ_b). Each type of basis functions forms a complete set, when an upper limit N_n ($n=2,4,b$) of the summation is infinite. The G_n's are constructed from the set

$$\{(x_1x_2x_3x_4)^\beta x_1^{n_1}x_2^{n_2}x_3^{n_3}x_4^{n_4}\}$$

which obviously forms a complete set. First, it is transformed into

$$\{(x_1x_2x_3x_4)^\beta(x_{13}^-)^{n_1}(x_{13}^+)^{n_2}(x_{24}^+)^{n_3}(x_{24}^-)^{n_4}\}.$$

Next, a factor $(x_{13}^+)^{n_2}(x_{24}^+)^{n_3}$ in the set is expanded in terms of $(x_{13}^+x_{24}^+)^n$ and $(x_{13}^+x_{24}^+)^nx_{13}^+$, where $x_{13}^++x_{24}^+=1$; see Appendix B for the expansion. The final form is Eq. (3.6), in which the number of summations has been reduced from 4 to 3. This is a merit of this form. Another merit is that the symmetry for an interchange of x_1 and x_3 (x_2 and x_4) is easily imposed on ψ_4 by taking either even or odd n_1 (n_3). Similar consideration is made for f_n and F_n.

B. Numerical results

In general, M calculated with the variational method depends on N_α ($\alpha=2,4,b$), which characterizes the size of the space spanned by the basis functions, unless the space is large enough to yield an accurate M. In the present calculation, the space would be sufficiently large, since the dependence is very weak, owing to the effective choice of basis functions. This is shown in Fig. 1 for SU(2) meson. Figure 1(a) represents N_2 dependences of the lightest mass (M_1) and the second lightest one (M_2), while Fig. 1(b) does their N_4 dependences. Hereafter, m and M are presented in units of $\sqrt{g^2N/2\pi}$. In the case of $m=10^{-4}$, M_1 and M_2 converge at $(N_2,N_4)=(4,4)$, while the baryonic mass (M_b) does at $N_b=2$. Our full-fledged calculations are then done with $(N_2,N_4)=(4,4)$ for meson and with $N_b=2$ for baryon.

The m dependence of hadron masses obtained with full-fledged calculations is shown in Table I and Fig. 2 for both SU(2) and SU(3). There are two mesonic and one baryonic bound states in the range $m<0.1$. The lightest meson is composed predominantly of valence quarks; in the case of SU(2), for example, $P_2=98.3\%$ and $P_4=1.7\%$ at $m=10^{-4}$, where P_2 (P_4) is a probability of being in the $q\bar{q}$ ($qq\bar{q}\,\bar{q}$) state. The lightest mesonic state is odd under charge conjugation, because the two-body ($q\bar{q}$) component is symmetric under $x_1\leftrightarrow x_2$. The second

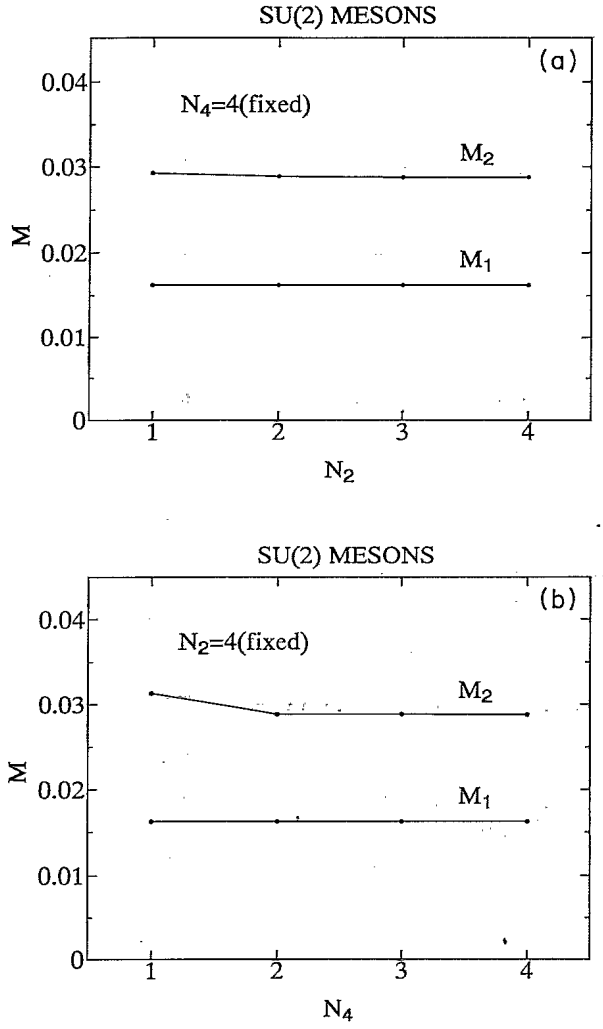

FIG. 1. Masses of the lightest (M_1) and the second lightest (M_2) SU(2) mesons are shown as a function of one of the parameters, which characterize the size of the space spanned by the basis functions [see Eqs. (3.1)–(3.3)]; (a) N_2 is varied, while N_4 is fixed, and (b) N_4 is varied, while N_2 is fixed. Here the masses are presented in units of $\sqrt{g^2N/2\pi}$. The lines are intended to guide the eye.

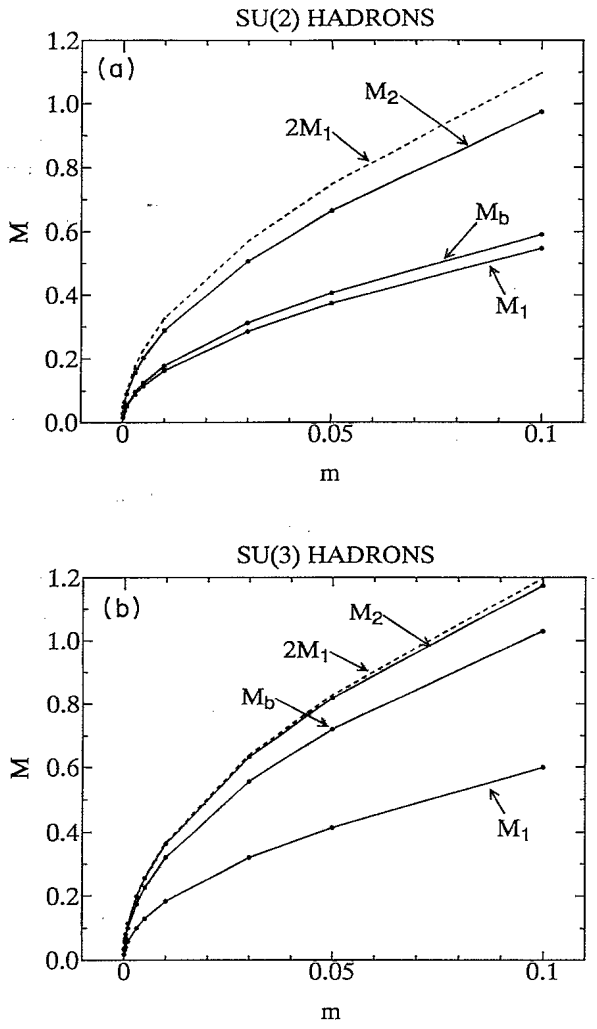

FIG. 2. Masses of the lowest two mesonic (M_1 and M_2) and one baryonic (M_b) bound states, obtained with the full-fledged calculations, are presented in units of $\sqrt{g^2N/2\pi}$ as a function of the quark mass m, (a) for SU(2) and (b) for SU(3). They are shown as points and the solid line guides the eye. The two-body decay threshold $2M_1$ is also shown by the dashed line.

TABLE I. Calculated masses of the SU(2) and SU(3) hadronic bound states M_1, M_2, and M_b are tabulated for various values of the quark mass m. Here all the masses are given in units of $\sqrt{g^2N/2\pi}$.

	$N=2$			$N=3$		
m	M_1	M_2	M_b	M_1	M_2	M_b
0.0001	0.016 26	0.028 80	0.017 73	0.018 49	0.036 66	0.032 03
0.0005	0.036 35	0.064 14	0.039 64	0.041 34	0.081 42	0.071 62
0.0010	0.051 41	0.090 67	0.056 08	0.058 46	0.114 95	0.101 30
0.0050	0.115 12	0.203 25	0.125 69	0.130 53	0.256 74	0.226 60
0.0100	0.163 17	0.288 58	0.178 25	0.184 43	0.363 36	0.320 62
0.0500	0.374 14	0.665 80	0.407 48	0.414 86	0.819 63	0.721 06
0.1000	0.549 15	0.974 61	0.591 64	0.598 95	1.174 76	1.030 14

lightest state is, on the other hand, highly relativistic in the sense that $P_2 \sim P_4$; in the case of SU(2), for example $P_2 = 42.9\%$ and $P_4 = 57.1\%$ at $m = 10^{-4}$. This state is even under charge conjugation, since the two-body piece is antisymmetric under $x_1 \leftrightarrow x_2$.

The lightest mesonic mass is calculated also with the bosonization [2,4], the lattice theory [3,4], and the DLCQ method [7]. These results are compared with ours, in Fig. 3, for SU(2). The lattice calculation has much larger errors than ours, but both are consistent with each other within the errors. The DLCQ result matches well to ours at $m > 0.3$, but it lies too low at $m < 0.2$; for example the discrepancy is about 30% at $m = 0.088$. The substantial discrepancy at strong coupling may be because the resolution parameter $K \sim 10$ taken in the DLCQ calculation is too small; note that the DLCQ result shown in Fig. 3 is the physical mass (M_1 at $K = \infty$) extrapolated from M_1 computed at some different K around 10. In the strong coupling region such as $m < 0.2$, $\psi_2(x)$ rapidly goes down from 1 to 0 as x approaches 0 or 1. The strong x dependence near the ends cannot be reproduced by the DLCQ wave function computed at the small K; Hornbostel [23] estimates from the x dependence that K should be larger than 10^6 at $m = 0.088$. Thus M_1 measured at the small K is considered to contain large errors. The errors, however, seems to be reduced to a considerable extent by the extrapolation.

The result of the bosonization overshoots not only ours but also the one of the lattice calculation in Fig. 3. Our result behaves as $m^{1/2}$, while the result of the bosonization as $m^{2/3}$. The lattice calculation seems to support $m^{1/2}$. The result of the bosonization is derived with a method of Dashen, Hasslacher, and Neveu [24] based on the WKB approximation. For ratios of mesonic masses to a baryonic mass, Dashen, Hasslacher, and Neveu have checked their result against several nontrivial orders of perturbation and conjecture that it is exact, but they do not claim to be able to compute hadronic masses themselves exactly. The result of the bosonization in Fig. 3 is thus not expected to be exact. Therefore we may conclude that the correct m dependence of the mesonic mass is $m^{1/2}$, although the m dependence has been believed to be $m^{2/3}$ so far. On the other hand, we may assume that the result of Dashen, Hasslacher, and Neveu is indeed correct for the ratios. This assumption was first made by Coleman [25], when he analyzed the massive Schwinger model by applying the result of Dashen, Hasslacher, and Neveu to the bosonic form of the theory.

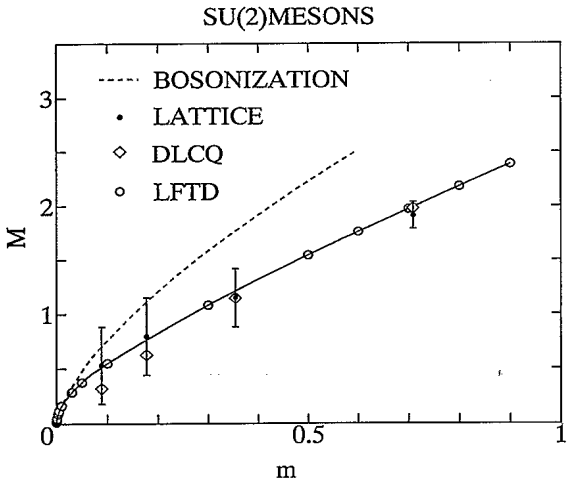

FIG. 3. Some theoretical results for a mass of the lowest SU(2) meson are presented in units of $\sqrt{g^2N/2\pi}$ as a function of m; the result of our full-fledged calculation are shown by open circles, the DLCQ result [7] by diamonds and the bosonization result [2,4] by a dashed line. The lattice estimates [4] are shown as points with error bars.

Figure 2 shows that all hadronic masses calculated with LFTD behave like $m^{1/2}$ as $m \to 0$. Ratios $M_1/2M_b$ and $M_2/2M_b$ at small m, say $m = 10^{-4}$, are 0.4585 and 0.8122 for SU(2) and 0.2886 and 0.5722 for SU(3), while the corresponding results, $\sin\{\pi n/2(2N-1)\}$ $(n = 1, 2)$, of the bosonization [2] in the massless limit are 0.5000 and 0.8660 for SU(2) and 0.3090 and 0.5877 for SU(3). The two types of results are identical within an error of $\sim 10\%$ for SU(2) and of $\sim 5\%$ for SU(3). In general, our calculation of the baryonic mass is relatively inaccurate compared with that of the mesonic masses, since the truncated Fock space is smaller in the baryonic case than in the mesonic one; to be precise, only the valence (N-body) state is included in the baryonic Fock space, while the mesonic Fock space is composed of both the two-body ($q\bar{q}$) and the four-body ($qq\bar{q}\,\bar{q}$) state. According to numerical calculations for SU(2), M_1 is reduced by $\sim 10\%$, when the Fock space is extended from the two-body subspace to the two-body plus four-body one. It is very likely that such a reduction takes place also for M_b, since the ES equation for M_b is very similar to that for M_1 in the SU(2) case. Thus, the $\sim 10\%$ error for SU(2) is considered to come from the fact that the $(N+2)$-body state is not included in the baryonic Fock space. For the SU(3) case, on the other hand, it is confirmed numerically that M_1 is little changed by the extension of the two-body subspace to the two-body plus four-body subspace. This is because g is decreased as N increases. It is then likely that M_b is also unchanged by a similar extension of the baryonic Fock space from the N-body subspace to the N-body plus $(N+2)$-body one. Therefore, we may conclude that our full-fledged calculations for SU(3) are accurate for M_b as well as M_1. An unsettled problem is what causes the $\sim 5\%$ error for SU(3). This will be discussed in Sec. IV.

The approximate solutions [Eqs. (2.25) and (2.26)] to M_1 and M_b are compared with numerical ones obtained with the full-fledged calculations, in two cases of SU(2) and SU(3). For SU(2), the approximate M_1 is exactly equal to the approximate M_b, as shown in Eqs. (2.25) and (2.26). They are depicted by a single dashed line in Fig. 4(a), and compared with the numerical solutions for M_1 (solid line) and for M_b (dot-dashed line). The approximate solution matches well to the numerical results for both M_1 and M_b. For SU(3) in Fig. 4(b), the approximate solutions well reproduce the numerical ones, for both M_1 and M_b, at $m < 0.1$. The agreement would be seen also at N larger than 3; this is true at least for M_1 [see Fig. 5(a)]. The N dependence of M_1 and M_b is

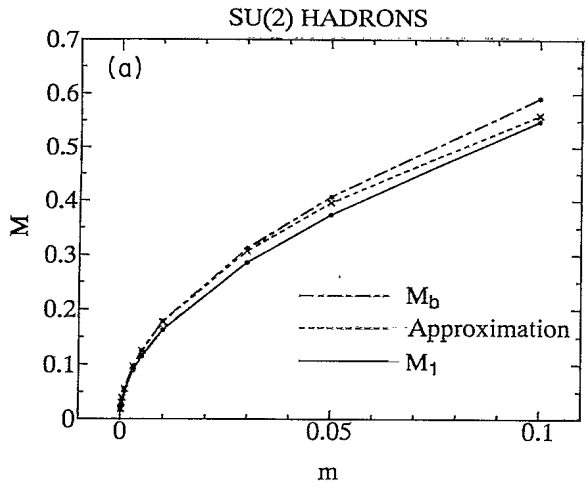

FIG. 4. Numerical and approximate masses of the lowest mesonic (M_1) and baryonic (M_b) states are shown in units of $\sqrt{g^2N/2\pi}$ as a function of the quark mass m. (a) For the SU(2) case, the numerical solutions to M_1 and M_b are graphed with the solid and dot-dashed lines, respectively, while the approximate ones to both of them are degenerate and therefore graphed with a dashed line. (b) For the SU(3) case, the numerical and the approximate solutions are graphed with the solid and dashed lines, respectively, for both M_1 and M_b.

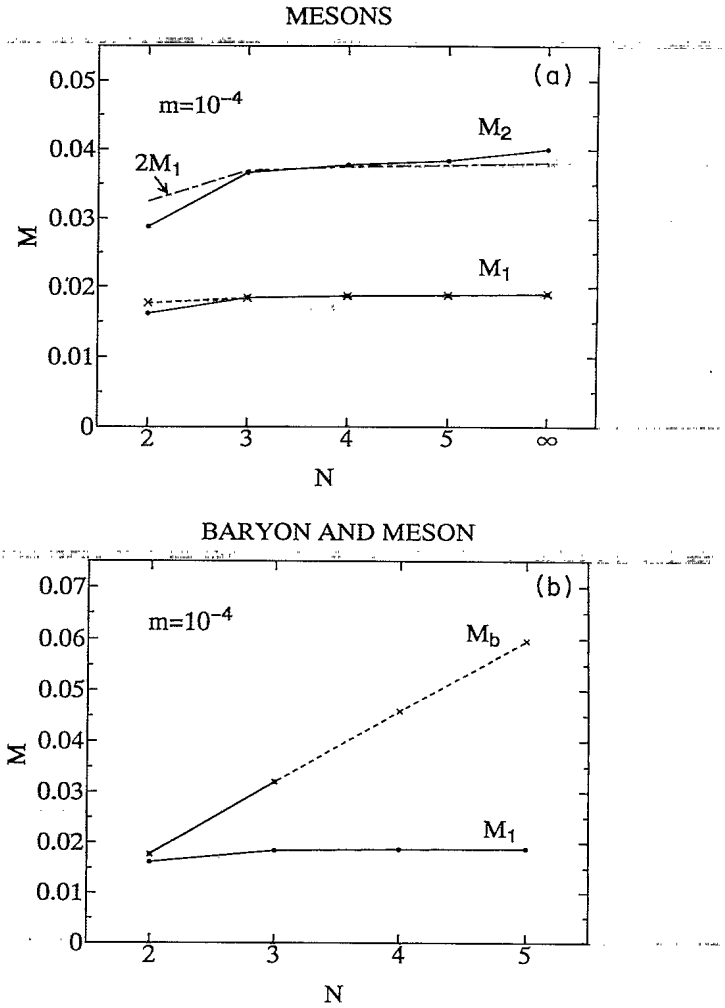

FIG. 5. Numerical solutions to (a) the second lightest mesonic and (b) the lightest baryonic masses, calculated for SU(N) by adopting a quark mass $m = 10^{-4}$, are shown by the solid lines as a function of N in comparison to that of the lightest meson. The approximate solutions, which are available only for the lightest meson and baryon, are shown by the dashed lines in (a) and (b), respectively. The two-body decay threshold, $2M_1$, is also shown by the dot-dashed line in (a). Here all the masses are given in units of $\sqrt{g^2N/2\pi}$.

thus obtained accurately with the approximate solutions, as long as $m^2 \ll 1$.

The N-dependence of M_1 and M_2 is shown at $m = 10^{-4}$, in Fig. 5(a), where N is varied widely from 2 to ∞. The approximate solution to M_1 (dashed line) well simulates the numerical solution (solid line). As expected from the weak N dependence of the approximate M_1, M_1 at small N is close to that at $N \to \infty$ (the lightest 't Hooft mass). The second mass is below the threshold ($2M_1$) for $N = 2$ and 3 but not for $N \geq 4$. The second mesonic state is thus bound only for such small N. The existence of the second bound state at small N is unpredictable from the leading order in $1/N$, since the state becomes unbound at $N \to \infty$. The $1/N$ expansion thus works well for the first mesonic mass, but not for the second mass.

The N dependence of M_b is shown in Fig. 5(b). The approximate solution to M_b (solid line) well reproduces the numerical result (dashed line) for $N = 2$ and 3. In a $1/N$ expansion of M_b the leading is $O(N)$ [16–18]. A ratio of M_b at $N = 3$ to that at $N = 2$ is, however, 1.807 and larger than $\frac{3}{2}$. This indicates that the higher-order terms are not negligible for such small N.

Figure 6 shows the m-dependence of mesonic masses in the large N limit. In this limit, the two- and four-body sectors of the ES equations are decoupled from each other so that all states appear as either two- or four-body states. Obviously, all the two-body states (the 't Hooft solutions) are bound. In Fig. 6, on the other hand, the lightest four-body state is above the threshold ($2M_1$),

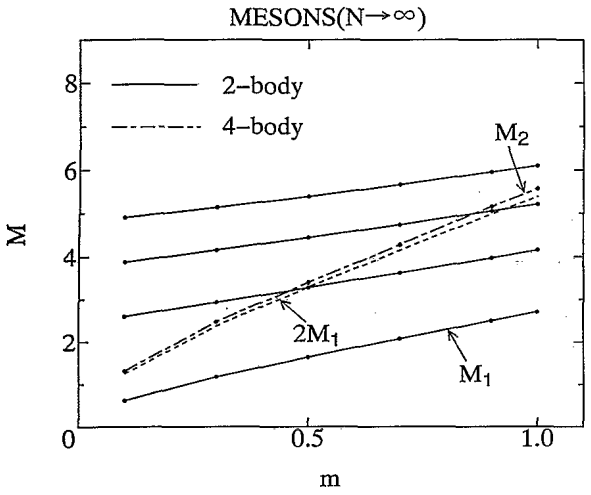

FIG. 6. Masses of the lowest four two-body and a four-body SU(N) mesonic states in the large N limit are shown as a function of the quark mass m by the solid lines and the dot-dashed line, respectively. The two-body decay threshold, $2M_1$, is also shown by the dashed line. Note that all the masses are given in units of $\sqrt{g^2N/2\pi}$.

where M_1 is the mass of the lightest two-body bound state. All the four-body states are thus unbound. This is understandable from the statement [14] based on the $1/N$ expansion that two mesons (two q-$\bar{q}$ pairs) do not interact in the limit.

IV. DISCUSSIONS

Some unsettled problems are discussed. (1) As shown in Sec. III B, our results for $M_1/2M_b$ and $M_2/2M_b$ deviate from the prediction of the bosonization [2] by $\sim 5\%$ in the case of SU(3). A problem in the comparison is that the two types of results are obtained at different m; the results of the bosonization are done at $m = 0$ and ours at $m = 10^{-4}$. In the bosonization, the color-singlet bosonic field is coupled with the nonsinglet fields. The nonsinglet fields are, however, neglected in the bosonic form of the Hamiltonian. The neglect seems to induce an error of $O(M_S/M_{NS})$, where M_S (M_{NS}) is a mass of the lowest state produced by the singlet (nonsinglet) field. We intuitively think that the nonsinglet fields can generate singlet states as a result of their superposition, but it is not clear from the bosonic form of the Hamiltonian, which does not possess the SU(N) symmetry explicitly. The M_{NS} seems to be of order 1 independently of m/g, since the nonsinglet fields have mass terms of order 1. The M_S, on the other hand, tends to zero in the massless limit ($m/g \to 0$). The result of the bosonization is then correct in the massless limit. At $m = 10^{-4}$, it has an error of $O(M_S/M_{NS}) \sim O(M_1/M_{NS}) \sim 10^{-2}$. This error is a possible origin of the discrepancy between the two types of results.

(2) A natural expectation for the Tamm-Dancoff approximation is that it works best at weak coupling rather than strong coupling. The present work, however, points out that it works in both the regions. As an evidence, the lightest meson consists only of a q-$\bar{q}$ pair in the limit of strong coupling, so that the meson has small four-body components even for large but finite g. Similar results are seen in the massive Schwinger model [13,15]. It is not obvious whether the approximation still works in four dimensions, since the four-dimensional QCD Hamiltonian is much more complicated than the two-dimensional one.

(3) Our truncated Fock space consists of the two- and four-body states in the mesonic case. Further inclusion of six-body states would produce the third mesonic bound state at strong coupling. This may be expected from the following considerations in the limit of strong coupling: The bosonization [2] predicts for SU(N) meson that there appear $2N-1$ massless bound states, and DLCQ [7] does that there are many massless mesonic states and the nth state consists of n components from two body to $2n$ body.

(4) In the massive Schwinger model, the axial symmetry is anomalous and the light-cone Hamiltonian involves a force induced by the so-called annihilation diagrams where a q-$\bar{q}$ pair annihilates into an instantaneous gluon at a vertex, while another pair is created at the second vertex [15]. The force generates a term $2\int_0^1 dx\,\psi(x,1-x)$ in the ES equation for "η" (isosinglet) mass, but not for "π" (isotriplets) mass. The term splits the η mass from the π mass; especially in the chiral limit, the η mass keeps a finite value, but the π mass vanishes. In the present model, on the other hand, the axial symmetry is not anomalous, but the annihilation force is still in P^-. In this case, the force does not generate any term that makes η massive in the chiral limit. Thus, the η-π splitting [the U(1) problem] may not be resolved simply as a matter of the annihilation force.

Throughout this work, we conclude that LFTD is a powerful tool for computing nonperturbative quantities such as hadronic masses. We believe that LFTD is more useful than the $1/N$ expansion and the bosonization, which are valid only in a particular situation such as the large N limit or the large g/m limit.

ACKNOWLEDGMENTS

We would like to acknowledge stimulating conversations with our colleagues, in particular K. Harada. We are grateful to K. Hornbostel for his quick reply to our question on his work.

APPENDIX A: EINSTEIN-SCHRÖDINGER EQUATIONS

A set of coupled integral equations is obtained by applying the Hamiltonian (2.14) to the states (2.15) and (2.18). For four-body wave functions, $\sum_{i=1}^4 x_i = 1$. It reads, for SU(N) mesons,

$$
\begin{aligned}
M^2\psi_2(x,1-x) = {} & \left(m^2 - \frac{N^2-1}{2N}\frac{g^2}{\pi}\right)\left(\frac{1}{x}+\frac{1}{1-x}\right)\psi_2(x,1-x) - \frac{N^2-1}{2N}\frac{g^2}{\pi}\int_0^1 dy \frac{\psi_2(y,1-y)}{(x-y)^2} \\
& + \frac{(N-1)\sqrt{2(N+1)}}{2N}\frac{g^2}{\pi}\int_0^1 dy_1\, dy_2\, dy_3 \\
& \times\left\{\psi_A(x,y_1,y_2,y_3)\frac{\delta(y_1+y_2+y_3-(1-x))}{[y_3-(1-x)]^2} - \psi_A(y_1,y_2,y_3,1-x)\frac{\delta(y_1+y_2+y_3-x)}{(y_1-x)^2}\right\} \\
& + \frac{(N+1)\sqrt{2(N-1)}}{2N}\frac{g^2}{\pi}\int_0^1 dy_1 dy_2 dy_3 \\
& \times\left\{\psi_S(x,y_1,y_2,y_3)\frac{\delta(y_1+y_2+y_3-(1-x))}{[y_3-(1-x)]^2} - \psi_S(y_1,y_2,y_3,1-x)\frac{\delta(y_1+y_2+y_3-x)}{(y_1-x)^2}\right\}, \qquad \text{(A1)}
\end{aligned}
$$

$$
\begin{aligned}
M^2\psi_A(x_1,x_2,x_3,x_4) = {} & \left(m^2 - \frac{N^2-1}{2N}\frac{g^2}{\pi}\right)\left(\sum_{i=1}^4 \frac{1}{x_i}\right)\psi_A(x_1,x_2,x_3,x_4) \\
& + \frac{(N-1)\sqrt{2(N+1)}}{8N}\frac{g^2}{\pi}\left\{\left[\frac{1}{(x_2+x_3)^2} - \frac{1}{(x_3+x_4)^2}\right]\psi_2(x_1,1-x_1)\right. \\
& + \left[\frac{1}{(x_3+x_4)^2} - \frac{1}{(x_1+x_4)^2}\right]\psi_2(1-x_2,x_2) + \left[\frac{1}{(x_1+x_4)^2} - \frac{1}{(x_1+x_2)^2}\right]\psi_2(x_3,1-x_3) \\
& \left. + \left[\frac{1}{(x_1+x_2)^2} - \frac{1}{(x_2+x_3)^2}\right]\psi_2(1-x_4,x_4)\right\} \\
& + \frac{N-1}{2N}\frac{g^2}{\pi}\int_0^1 dy_1 dy_2\left\{\frac{\delta(x_1+x_3-y_1-y_2)}{(x_1-y_1)^2}\psi_A(y_1,x_2,y_2,x_4)\right. \\
& \left. + \frac{\delta(x_2+x_4-y_1-y_2)}{(x_2-y_1)^2}\psi_A(x_1,y_1,x_3,y_2)\right\} \\
& + \frac{N-1}{4N}\frac{g^2}{\pi}\int_0^1 dy_1\, dy_2\left\{\frac{\delta(x_1+x_2-y_1-y_2)}{(x_1+x_2)^2}\psi_A(y_1,y_2,x_3,x_4)\right. \\
& - \frac{\delta(x_1+x_4-y_1-y_2)}{(x_1+x_4)^2}\psi_A(y_1,y_2,x_3,x_2) - \frac{\delta(x_3+x_2-y_1-y_2)}{(x_3+x_2)^2}\psi_A(y_1,y_2,x_1,x_4) \\
& \left. + \frac{\delta(x_3+x_4-y_1-y_2)}{(x_3+x_4)^2}\psi_A(y_1,y_2,x_1,x_2)\right\} \\
& - \frac{(N-1)(N+2)}{4N}\frac{g^2}{\pi}\int_0^1 dy_1\, dy_2\left\{\frac{\delta(x_1+x_2-y_1-y_2)}{(x_1-y_1)^2}\psi_A(y_1,y_2,x_3,x_4)\right. \\
& - \frac{\delta(x_1+x_4-y_1-y_2)}{(x_1-y_1)^2}\psi_A(y_1,y_2,x_3,x_2) - \frac{\delta(x_3+x_2-y_1-y_2)}{(x_3-y_1)^2}\psi_A(y_1,y_2,x_1,x_4) \\
& \left. + \frac{\delta(x_3+x_4-y_1-y_2)}{(x_3-y_1)^2}\psi_A(y_1,y_2,x_1,x_2)\right\} \\
& - \frac{\sqrt{(N+1)(N-1)}}{4N}\frac{g^2}{\pi}\int_0^1 dy_1\, dy_2 \\
& \times\left\{\delta(x_1+x_2-y_1-y_2)\psi_S(y_1,y_2,x_3,x_4)\times\left[\frac{1}{(x_1+x_2)^2} + \frac{N}{(x_1-y_1)^2}\right]\right. \\
& -\delta(x_1+x_4-y_1-y_2)\psi_S(y_1,y_2,x_3,x_2)\left[\frac{1}{(x_1+x_4)^2} + \frac{N}{(x_1-y_1)^2}\right] \\
& -\delta(x_3+x_2-y_1-y_2)\psi_S(y_1,y_2,x_1,x_4)\left[\frac{1}{(x_3+x_2)^2} + \frac{N}{(x_3-y_1)^2}\right] \\
& \left. +\delta(x_3+x_4-y_1-y_2)\psi_S(y_1,y_2,x_1,x_2)\left[\frac{1}{(x_3+x_4)^2} + \frac{N}{(x_3-y_1)^2}\right]\right\}, \qquad \text{(A2)}
\end{aligned}
$$

$$
\begin{aligned}
M^2\psi_S(x_1,x_2,x_3,x_4) = &\left(m^2-\frac{N^2-1}{2N}\frac{g^2}{\pi}\right)\left(\sum_{i=1}^{4}\frac{1}{x_i}\right)\psi_S(x_1,x_2,x_3,x_4)+\frac{(N+1)\sqrt{2(N-1)}}{8N}\frac{g^2}{\pi}\\
&\times\left\{\left[\frac{1}{(x_2+x_3)^2}+\frac{1}{(x_3+x_4)^2}\right]\psi_2(x_1,1-x_1)-\left[\frac{1}{(x_3+x_4)^2}+\frac{1}{(x_1+x_4)^2}\right]\psi_2(1-x_2,x_2)\right.\\
&\left.+\left[\frac{1}{(x_1+x_4)^2}+\frac{1}{(x_1+x_2)^2}\right]\psi_2(x_3,1-x_3)-\left[\frac{1}{(x_1+x_2)^2}+\frac{1}{(x_2+x_3)^2}\right]\psi_2(1-x_4,x_4)\right\}\\
&-\frac{N+1}{2N}\frac{g^2}{\pi}\int_0^1 dy_1\,dy_2\left\{\frac{\delta(x_1+x_3-y_1-y_2)}{(x_1-y_1)^2}\psi_S(y_1,x_2,y_2,x_4)\right.\\
&\left.+\frac{\delta(x_2+x_4-y_1-y_2)}{(x_2-y_1)^2}\psi_S(x_1,y_1,x_3,y_2)\right\}\\
&+\frac{N+1}{4N}\frac{g^2}{\pi}\int_0^1 dy_1\,dy_2\left\{\frac{\delta(x_1+x_2-y_1-y_2)}{(x_1+x_2)^2}\psi_S(y_1,y_2,x_3,x_4)\right.\\
&+\frac{\delta(x_1+x_4-y_1-y_2)}{(x_1+x_4)^2}\psi_S(y_1,y_2,x_3,x_2)\\
&\left.+\frac{\delta(x_3+x_2-y_1-y_2)}{(x_3+x_2)^2}\psi_S(y_1,y_2,x_1,x_4)+\frac{\delta(x_3+x_4-y_1-y_2)}{(x_3+x_4)^2}\psi_S(y_1,y_2,x_1,x_2)\right\}\\
&-\frac{(N+1)(N-2)}{4N}\frac{g^2}{\pi}\int_0^1 dy_1\,dy_2\left\{\frac{\delta(x_1+x_2-y_1-y_2)}{(x_1-y_1)^2}\psi_S(y_1,y_2,x_3,x_4)\right.\\
&+\frac{\delta(x_1+x_4-y_1-y_2)}{(x_1-y_1)^2}\psi_S(y_1,y_2,x_3,x_2)+\frac{\delta(x_3+x_2-y_1-y_2)}{(x_3-y_1)^2}\psi_S(y_1,y_2,x_1,x_4)\\
&\left.+\frac{\delta(x_3+x_4-y_1-y_2)}{(x_3-y_1)^2}\psi_S(y_1,y_2,x_1,x_2)\right\}\\
&-\frac{\sqrt{(N+1)(N-1)}}{4N}\frac{g^2}{\pi}\int_0^1 dy_1dy_2\\
&\times\left\{\delta(x_1+x_2-y_1-y_2)\psi_A(y_1,y_2,x_3,x_4)\left[\frac{1}{(x_1+x_2)^2}+\frac{N}{(x_1-y_1)^2}\right]\right.\\
&+\delta(x_1+x_4-y_1-y_2)\psi_A(y_1,y_2,x_3,x_2)\left[\frac{1}{(x_1+x_4)^2}+\frac{N}{(x_1-y_1)^2}\right]\\
&+\delta(x_3+x_2-y_1-y_2)\psi_A(y_1,y_2,x_1,x_4)\left[\frac{1}{(x_3+x_2)^2}+\frac{N}{(x_3-y_1)^2}\right]\\
&\left.+\delta(x_3+x_4-y_1-y_2)\psi_A(y_1,y_2,x_1,x_2)\left[\frac{1}{(x_3+x_4)^2}+\frac{N}{(x_3-y_1)^2}\right]\right\}. \qquad \text{(A3)}
\end{aligned}
$$

The baryonic Fock space has been described only with the N-body component so far in this paper. To study a role of the higher Fock components, we then add a $(N+2)$-body component to the space. The component is constructed, for SU(2), as

$$
\begin{aligned}
|\text{baryon}\rangle_{N+2} = &\frac{1}{2}\int_0^{\mathcal{P}}\prod_{i=1}^{4}\frac{dk_i}{\sqrt{2\pi k_i}}\delta\left(\mathcal{P}-\sum_{i=1}^{4}k_i\right)\psi_M(k_1,k_2,k_3,k_4)\\
&\times[b_1^\dagger(k_1)b_2^\dagger(k_2)b_1^\dagger(k_3)d_1^\dagger(k_4)-b_2^\dagger(k_1)b_1^\dagger(k_2)b_2^\dagger(k_3)d_2^\dagger(k_4)]|0\rangle, \qquad \text{(A4)}
\end{aligned}
$$

with the symmetry

$$
\psi_M(k_1,k_2,k_3,k_4) = -\psi_M(k_3,k_2,k_1,k_4). \qquad \text{(A5)}
$$

In the derivation of Eq. (A4), the $(N+2)$-body wave function $\psi(k_1,k_2,k_3,k_4)$ has been classified with irreducible representations of the symmetric group:

$$
\psi(k_1,k_2,k_3,k_4) = \psi_{\text{sym}}(k_1,k_2,k_3,k_4)+\psi_{\text{ant}}(k_1,k_2,k_3,k_4)+\psi_M(k_1,k_2,k_3,k_4), \qquad \text{(A6)}
$$

where

$$\psi_{\rm sym}(k_1,k_2,k_3,k_4)= \mathcal{S}_{123}\psi(k_1,k_2,k_3,k_4),$$
$$\psi_{\rm ant}(k_1,k_2,k_3,k_4)= \mathcal{A}_{123}\psi(k_1,k_2,k_3,k_4),$$
$$\psi_M(k_1,k_2,k_3,k_4)= \tfrac{1}{3}[2\psi(k_1,k_2,k_3,k_4)-\psi(k_2,k_3,k_1,k_4)-\psi(k_3,k_1,k_2,k_4)], \tag{A7}$$

Here $\mathcal{S}_{123}$ is the symmetrizer of momenta k_1, k_2, and k_3, while $\mathcal{A}_{123}$ is the antisymmetrizer. Only the mixed symmetry ψ_M can survive under the condition that $Q^2|\Psi\rangle = 0$ and then appears in Eq. (A4). The $(N+2)$-body wave function can be constructed straightforwardly for arbitrary N. The coupled equations are then, for the SU(2) baryon,

$$M^2\psi_b(x,1-x) = \left(m^2-\frac{3g^2}{4\pi}\right)\left(\frac{1}{x}+\frac{1}{1-x}\right)\psi_b(x,1-x) - \frac{3g^2}{4\pi}\int_0^1 dy\frac{\psi_b(y,1-y)}{(x-y)^2} + \frac{g^2}{2\pi}\int_0^1 dy_1\,dy_2\,dy_3$$
$$\times\left\{\delta(y_1+y_2+y_3-x)\psi_M(y_1,1-x,y_2,y_3)\frac{1}{(x-y_1)^2}\right.$$
$$\left.-2\delta(y_1+y_2+y_3-x)\psi_M(1-x,y_1,y_2,y_3)\left[\frac{1}{2(x-y_1)^2}+\frac{1}{(x-y_2)^2}\right]\right\}, \tag{A8}$$

$$M^2\psi_M(x_1,x_2,x_3,x_4) = \left(m^2-\frac{3g^2}{4\pi}\right)\left(\sum_{i=1}^4\frac{1}{x_i}\right)\psi_M(x_1,x_2,x_3,x_4) + \frac{g^2}{2\pi}\left\{\frac{1}{2}\left[\frac{1}{(x_3+x_4)^2}-\frac{1}{(x_1+x_4)^2}\right]\psi_b(x_2,1-x_2)\right.$$
$$\left.-\left[\frac{1}{(x_2+x_4)^2}+2\frac{1}{(x_3+x_4)^2}\right]\psi_b(x_1,1-x_1)+\left[\frac{1}{(x_2+x_4)^2}+2\frac{1}{(x_1+x_4)^2}\right]\psi_b(x_3,1-x_3)\right\}$$
$$-\frac{g^2}{2\pi}\int_0^1 dy_1\,dy_2\left\{\delta(x_1+x_2-y_1-y_2)\left[\frac{1}{2(x_1-y_1)^2}+\frac{1}{(x_1-y_2)^2}\right]\psi_M(y_1,y_2,x_3,x_4)\right.$$
$$+\delta(x_2+x_3-y_1-y_2)\left[\frac{1}{2(x_2-y_1)^2}+\frac{1}{(x_2-y_2)^2}\right]\psi_M(x_1,y_1,y_2,x_4)$$
$$\left.-\frac{1}{4}\delta(x_1+x_3-y_1-y_2)\left[\frac{1}{2(x_1-y_1)^2}-\frac{1}{(x_1-y_2)^2}\right]\psi_M(y_1,x_2,y_2,x_4)\right\}$$
$$+\frac{g^2}{2\pi}\int_0^1 dy_1\,dy_2\left\{\delta(x_1+x_4-y_1-y_2)\left[\frac{1}{4(x_1+x_4)^2}-\frac{1}{(x_1-y_1)^2}\right]\psi_M(y_1,x_2,x_3,y_2)\right.$$
$$+\delta(x_3+x_4-y_1-y_2)\left[\frac{1}{4(x_3+x_4)^2}-\frac{1}{(x_3-y_1)^2}\right]\psi_M(x_1,x_2,y_1,y_2)$$
$$+\delta(x_2+x_4-y_1-y_2)\left[\frac{1}{(x_2+x_4)^2}+\frac{1}{2(x_2-y_1)^2}\right]\psi_M(x_1,y_1,x_3,y_2)$$
$$+\delta(x_1+x_4-y_1-y_2)\left[\frac{1}{4(x_1+x_4)^2}+\frac{1}{2(x_1-y_1)^2}\right]\psi_M(x_2,y_1,x_3,y_2)$$
$$\left.+\delta(x_3+x_4-y_1-y_2)\left[\frac{1}{4(x_3+x_4)^2}+\frac{1}{(x_3-y_1)^2}\right]\psi_M(x_1,y_1,x_2,y_2)\right\}. \tag{A9}$$

Again, integrating Eq. (A8) over x leads to Eq. (2.22).

APPENDIX B: BASIS FUNCTIONS

The function $x^m(1-x)^n$ can be expanded in terms of $[x(1-x)]^k$ and $[x(1-x)]^l(1-2x)$:

$$x^m(1-x)^n = 2^{-|m-n|}\left\{\sum_{i=0({\rm even})}^{|m-n|}{}_{|m-n|}C_i\sum_{j=0}^{i/2}{}_{i/2}C_j(-4)^j[x(1-x)]^{\min(m,n)+j}\right.$$
$$\left.-\epsilon(m-n)\sum_{i=1({\rm odd})}^{|m-n|}{}_{|m-n|}C_i\sum_{j=0}^{[i/2]}{}_{[i/2]}C_j(-4)^j[x(1-x)]^{\min(m,n)+j}(1-2x)\right\}. \tag{B1}$$

APPENDIX C: MATRIX EIGENVALUE EQUATIONS

The following eigenvalue equations of matrix form are obtained from the coupled equations [Eqs. (A1)–(A3)] by sandwiching them with individual two- and four-body basis functions:

$$M^2 \begin{pmatrix} A^{(1)} & 0 & 0 \\ 0 & B^{(1)} & 0 \\ 0 & 0 & B^{(1)} \end{pmatrix} \begin{pmatrix} a \\ b \\ c \end{pmatrix} = \begin{pmatrix} H_{11} & H_{12} & H_{13} \\ H_{21} & H_{22} & H_{23} \\ H_{31} & H_{32} & H_{33} \end{pmatrix} \begin{pmatrix} a \\ b \\ c \end{pmatrix},$$

where

$$\begin{aligned} H_{11} &= \left(m^2 - \frac{N^2-1}{2N}\frac{g^2}{\pi}\right) A^{(2)} - \frac{N^2-1}{2N}\frac{g^2}{\pi} A^{(3)}, \\ H_{22} &= 2\left(m^2 - \frac{N^2-1}{2N}\frac{g^2}{\pi}\right)(B^{(2)} + B^{(3)}) \\ &\quad + \frac{N-1}{N}\frac{g^2}{\pi} B^{(4)} - \frac{(N-1)(N+2)}{N}\frac{g^2}{\pi} B^{(5)} \\ &\quad + \frac{N-1}{2N}\frac{g^2}{\pi}(B^{(6)} + B^{(7)}), \\ H_{33} &= 2\left(m^2 - \frac{N^2-1}{2N}\frac{g^2}{\pi}\right)(B^{(2)} + B^{(3)}) \\ &\quad + \frac{N+1}{N}\frac{g^2}{\pi} B^{(4)} - \frac{(N+1)(N-2)}{N}\frac{g^2}{\pi} B^{(5)} \\ &\quad - \frac{N+1}{2N}\frac{g^2}{\pi}(B^{(6)} + B^{(7)}), \end{aligned} \tag{C1}$$

$$\begin{aligned} H_{12} = H_{21}^T &= \frac{(N-1)\sqrt{2(N+1)}}{2N}\frac{g^2}{\pi}(C^{(1)} - C^{(2)}), \\ H_{13} = H_{31}^T &= \frac{(N+1)\sqrt{2(N-1)}}{2N}\frac{g^2}{\pi}(C^{(1)} - C^{(2)}), \\ H_{23} = H_{32}^T &= -\frac{\sqrt{(N+1)(N-1)}}{N}\frac{g^2}{\pi}(B^{(4)} + NB^{(5)}), \end{aligned}$$

$$\begin{aligned} {A^{(1)}}_{kl} &= \int_0^1 dx f_k(x) f_l(x), \\ {A^{(2)}}_{kl} &= \int_0^1 dx \frac{f_k(x) f_l(x)}{x(1-x)}, \\ {A^{(3)}}_{kl} &= \int_0^1 dx dy \frac{f_k(x) f_l(y)}{(x-y)^2}, \\ {B^{(1)}}_{kl} &= \int_{(4)} G_k(x_1,x_2,x_3,x_4) G_l(x_1,x_2,x_3,x_4), \\ {B^{(2)}}_{kl} &= \int_{(4)} G_k(x_1,x_2,x_3,x_4) \frac{1}{x_1} G_l(x_1,x_2,x_3,x_4), \\ {B^{(3)}}_{kl} &= \int_{(4)} G_k(x_1,x_2,x_3,x_4) \frac{1}{x_2} G_l(x_1,x_2,x_3,x_4), \end{aligned} \tag{C2}$$

$$\begin{aligned} {B^{(4)}}_{kl} &= \int_{(6)} G_k(x_1,x_2,x_3,x_4) \\ &\quad \times \frac{1}{(x_1+x_2)^2} G_l(y_1,y_2,x_3,x_4), \\ {B^{(5)}}_{kl} &= \int_{(6)} G_k(x_1,x_2,x_3,x_4) \\ &\quad \times \frac{1}{(x_1-y_1)^2} G_l(y_1,y_2,x_3,x_4), \\ {B^{(6)}}_{kl} &= \int_{(6)'} G_k(x_1,x_2,x_3,x_4) \\ &\quad \times \frac{1}{(x_1-y_1)^2} G_l(y_1,x_2,y_2,x_4), \\ {B^{(7)}}_{kl} &= \int_{(6)''} G_k(x_1,x_2,x_3,x_4) \\ &\quad \times \frac{1}{(x_2-y_1)^2} G_l(x_1,y_1,x_3,y_2), \\ {C^{(1)}}_{kl} &= \int_{(4)} f_k(x_1) \frac{1}{(x_2+x_3)^2} G_l(x_1,x_2,x_3,x_4), \\ {C^{(2)}}_{kl} &= \int_{(4)} f_k(1-x_4) \frac{1}{(x_2+x_3)^2} G_l(x_1,x_2,x_3,x_4), \end{aligned}$$

$$\begin{aligned} \int_{(4)} &\equiv \int_0^1 \prod_{i=1}^4 dx_i \, \delta\left(\sum_{i=1}^4 x_i - 1\right), \\ \int_{(6)} &\equiv \int_0^1 \prod_{i=1}^4 dx_i \, dy_1 \, dy_2 \, \delta\left(\sum_{i=1}^4 x_i - 1\right) \\ &\quad \times \delta(x_1 + x_2 - y_1 - y_2), \\ \int_{(6)'} &\equiv \int_0^1 \prod_{i=1}^4 dx_i \, dy_1 \, dy_2 \, \delta\left(\sum_{i=1}^4 x_i - 1\right) \\ &\quad \times \delta(x_1 + x_3 - y_1 - y_2), \\ \int_{(6)''} &\equiv \int_0^1 \prod_{i=1}^4 dx_i \, dy_1 \, dy_2 \, \delta\left(\sum_{i=1}^4 x_i - 1\right) \\ &\quad \times \delta(x_2 + x_4 - y_1 - y_2). \end{aligned} \tag{C3}$$

These integrals with no N dependence can be calculated analytically with the formulas collected in Ref. [15].

[1] G. 't Hooft, Nucl. Phys. **B75**, 461 (1974).
[2] P. Steinhardt, Nucl. Phys. **B176**, 100 (1980). This paper contains several typographical errors and numerical slips, and these are corrected in Eq. (27) of Ref. [4].
[3] C. J. Hamer, Nucl. Phys. **B121**, 159 (1977); **B132**, 542 (1978).
[4] C. J. Hamer, Nucl. Phys. **B195**, 503 (1982).
[5] T. Eller, H. C. Pauli, and S. Brodsky, Phys. Rev. D **35**, 1493 (1987).
[6] T. Eller and H. C. Pauli, Z. Phys. C **42**, 59 (1989).
[7] K. Hornbostel, S. Brodsky, and H. Pauli, Phys. Rev. D **41**, 3814 (1990). The heading is mislabeled in Table I: M/g should be replaced by $M^2/(g^2/\pi + m^2)$. We were informed of this by Dr. Hornbostel.
[8] F. Lentz, M. Thies, S. Levit, and K. Yazaki, Ann. Phys. (N.Y.) **208**, 1 (1991).
[9] C. M. Yung and C. J. Hamer, Phys. Rev. D **44**, 2598 (1991).
[10] R. J. Perry, A. Harindranath, and K. G. Wilson, Phys. Rev. Lett. **65**, 2959 (1990).
[11] I. Tamm, J. Phys. (Moscow) **9**, 449 (1945); S. M. Dancoff, Phys. Rev. **78**, 382 (1950); H. A. Bethe and F. D. Hoffman, *Mesons and Fields* (Row, Peterson, Evanston, 1955), Vol. II; E. M. Henley and W. Thirring, *Elementary Quantum Field Theory* (McGraw-Hill, New York, 1962).
[12] An extensive list of references on light-front physics by A. Harindranath (light.tex is available via anonymous ftp from public.mps. ohio-state.edu under the subdirectory tmp/infolight).
[13] Y. Mo and R. J. Perry, J. Comp. Phys. **108**, 159 (1993).
[14] S. Coleman, Commun. Math. Phys. **31**, 259 (1973).
[15] K. Harada, T. Sugihara, M. Taniguchi, and M. Yahiro, Phys. Rev. D **49**, 4226 (1994).
[16] G. 't Hooft, Nucl. Phys. **B72**, 461 (1974).
[17] E. Witten, Nucl. Phys. **B160**, 57 (1979).
[18] S. Coleman, *Aspects of Symmetry* (Cambridge University Press, London, 1985).
[19] R. J. Perry and A. Harindranath, Phys. Rev. D **43**, 4051 (1991).
[20] W. M. Zhang and A. Harindranath, Phys. Rev D **48**, 4868 (1993).
[21] H. Bergknoff, Nucl. Phys. **B122**, 215 (1977).
[22] M. Burkardt, Nucl. Phys. **A504**, 762 (1989).
[23] K. Hornbostel, Ph.D. thesis, Stanford University, 1988.
[24] R. Dashen, B. Hasslacher, and A. Neveu, Phys. Rev. D **11**, 3424 (1975).
[25] S. Coleman, Ann. Phys. **101**, 239 (1976).